Chapter 3

Analytical Modeling of Subthreshold Current and Subthreshold Swing of Graded-Channel Dual-Material Double-Gate MOSFETs

3.1 Introduction

The subthreshold current (SC) and subthreshold swing (SS) characteristics of the MOSFETs are very important for estimating their switching characteristics in CMOS technology based digital circuits and systems. The lower value of SC is always desirable since it causes the undesired static power loss even when the MOSFET based switches are in the OFF state [Yeh and Fossum (1995), Dubey *et al.* (2010b)]. On the other hand, the smallest possible values (ideally zero) of the SS is also desirable since it represents the slope of the switching signal at the transition from the ON-to-OFF state or OFF-to-ON state [Yen *et al.* (1992), Dubey *et al.* (2011), Tiwari and Jit (2010b)]. Thus after modeling the potential distribution and threshold voltage characteristics of the GCDMDG MOSFET proposed in Chapter-2, we will now develop the analytical models for the SC and SS of the device in the present chapter. The SC model has been developed by using the potential model developed for the GCDMDG MOSFETs in Chapter-2. The concept of effective current conduction path [Chen *et al.* (2002), Dey *et al.* (2008), Dubey *et al.* (2011)] in DG MOSFETs has been used to determine the SS in the device. All definitions of different device parameters considered in Chapter-2 will also be used in this chapter for the ease of understanding of the readers. Some of the results/expressions developed in Chapter-2 will

also be directly used in this chapter. The layout of the present chapter can be given as follows:

Sec. 3.2 deals with the modeling of the SC and SS of the GCDMDG MOSFET considered in Chapter-2. First we have modeled the SC using the potential function derived in Chapter-2. We have then modelled the effective subthreshold current conduction path (d_{eff}) parameter of the proposed device. The SS has been modelled in terms of the d_{eff} parameter. The model results regarding the variations of SC and SS with different device parameters have been discussed in Sec. 2.3. In this section, we have also compared our proposed model results with the ATLAS^{TM} simulation data to validate the theoretical models developed for the SC and SS. Finally, Sec. 2.4 includes the summary and conclusion of this chapter.

3.2 Model Derivation

The cross-sectional view of GCDMDG MOSFET considered for present study is shown in Fig. 3.1. Although, the device structure used in this chapter is same as considered in Chapter 2 (Fig. 2.1), it is redrawn here for the sake of easy understanding of the work carried out in this chapter. The silicon film thickness, gate oxide thickness and channel length of the device are denoted by t_{si}, t_{ox}, and L respectively. x and y axes of the device are taken same as used in Chapter 1. The graded channel region consists of two non-overlapped regions 1 and 2 of respective lengths L_1 and L_2 and uniform doping concentrations of N_{a1} and N_{a2} where $L = L_1 + L_2$ and $N_{a1} > N_{a2}$. For achieving the DMG structure, two different gate electrode materials with work functions ϕ_{m1} and ϕ_{m2} (where

$\phi_{m1} > \phi_{m2}$) are used over the channel regions 1 and 2 respectively as already discussed in Chapter 1.

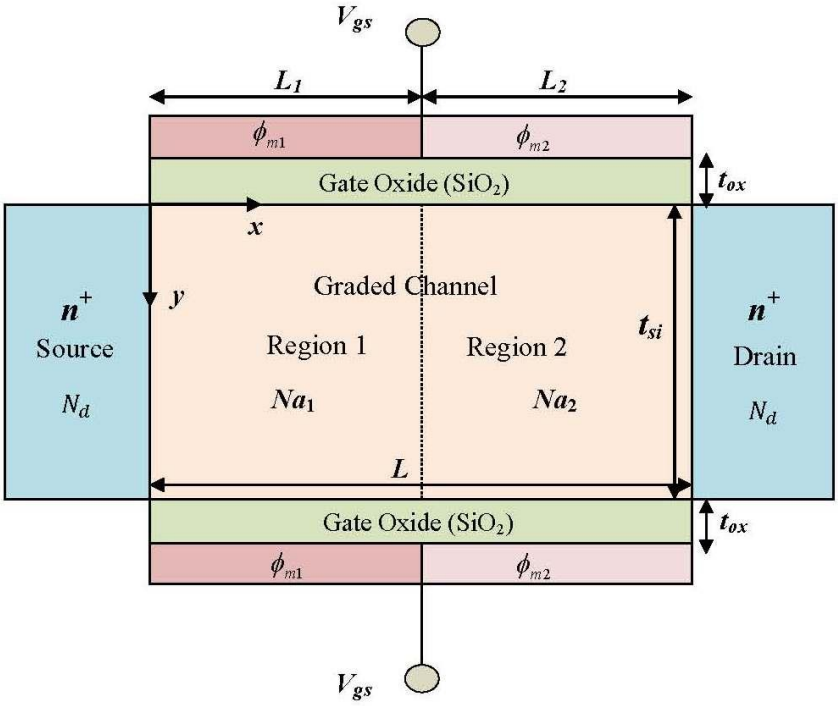

Fig. 3.1: Cross-sectional view of GCDMDG MOSFET

In the present chapter, symbolic presentation of all the device parameters have been kept same as used in Chapter 1. Further some of the results of Chapter 1 have been directly used for developing the models of SC and SS of the device under study.

3.2.1 Modeling of Subthreshold Current

Assuming diffusion the dominant current flow mechanism in the subthreshold regime of the device operation, SC of the device can be expressed as [Yeh and Fossum (1995), Dubey *et al.* (2010b)]

$$I_s = \int_0^{t_{si}} J_n(y)dy \tag{3.1}$$

where $J_n(y)$ shows current density and can be expressed as [Dubey *et al.* (2010b)],

$$J_n = \frac{qD_n n_{\min}(y)}{L_e}\left(1-\exp\left(\frac{-V_{ds}}{V_T}\right)\right) \tag{3.2}$$

where V_T is thermal voltage, L_e is effective-channel-length, D_n is diffusion-constant and

$$n_{\min}(y) = \frac{n_i^2}{N_{a1}}\exp\left(\left(\frac{\psi_{1\min}(y)}{V_T}\right)\right) \tag{3.3}$$

is the carrier-concentration at the virtual cathode with n_i as the intrinsic carrier-concentration and $\psi_{1\min}(y) = \psi_1(x_{\min,} y)$ is the minimum value of the 2D channel potential $\psi_1(x, y)$ at $x = x_{\min}$ under front gate i. e. in channel region 1 as discussed in Ref. [Goel *et al.* (2016).

Considering the depletion region widths at the source/channel and drain/channel junction as L_s and L_d respectively, the effective channel length can be expressed as [Dubey *et al.* (2010b)]

$$L_e = L - L_s - L_d + 2L_D \tag{3.4}$$

where L_D is the Debye length described by [Yeh and Fossum (1995), Dubey *et al.* (2010b)]

$$L_D = \left(\frac{\varepsilon_{si} V_T}{q N_{a1}} \right)^{1/2} \tag{3.5}$$

and L_s and L_d are expressed as [Dubey *et al.* (2011), Suzuki (2000)]

$$L_s \approx \left(\frac{2\varepsilon_{si} \left(V_{bi1} - \psi_{1\min}(y_{\min}) \right) N_d}{N_{a1}\left(N_{a1} + N_d \right)} \right)^{1/2} \tag{3.6}$$

$$L_d \approx \left(\frac{2\varepsilon_{si} \left(V_{bi2} + V_{ds} - \psi_{1\min}(y_{\min}) \right) N_d}{N_{a1}\left(N_{a1} + N_d \right)} \right)^{1/2} \tag{3.7}$$

where V_{ds} is drain-to-source voltage; V_{bi1} (V_{bi2}) is built-in potential at the source/channel (drain/channel) junction and $y_{\min}$ is obtained by

$$\left. \frac{\psi_{1\min}(y)}{\partial y} \right|_{y=y_{\min}} = 0 \tag{3.8}$$

Let us assume that the total channel region in the vertical direction ($0 \le y \le t_{si}$) is divided into two parts: front ($0 \le y \le y_{\min}$) and back ($y_{\min} \le y \le t_{si}$) regions. If current flowing through front and back regions are denoted by I_{sf} and I_{sb} respectively, then the total subthreshold current (SC) can be expressed as [Dubey *et al.* (2011)]

$$I_s = I_{sf} + I_{sb} \tag{3.9}$$

where I_{sf} and I_{sb} can be written as [Dubey *et al.* (2011)]

$$I_{sf} = C \left(\int_0^{y_m} \exp\left(\frac{\psi_{1\min}(y)}{V_T} \right) dy \right) \tag{3.10}$$

and

$$I_{sb} = C \left(\int_{y_m}^{t_{si}} \exp\left(\frac{\psi_{1\min}(y)}{V_T} \right) dy \right) \tag{3.11}$$

where $C = \frac{qD_n n_i^2}{N_{a1} L_e}\left(1 - \exp\left(\frac{-V_{ds}}{V_T}\right)\right)$ (3.12)

Following the methodology of Dey *et al.* [Dey *et al.* (2008)], Eq.(3.10) and Eq.(3.11) can be written as

$$I_{sf} = \frac{CV_T}{E_F}\left(\exp\left(\frac{\psi_{1\min}(y_m)}{V_T}\right) - \exp\left(\frac{\psi_{1\min}(0)}{V_T}\right)\right) \tag{3.13}$$

$$I_{sb} = \frac{CV_T}{E_b}\left(\exp\left(\frac{\psi_{1\min}(t_{si})}{V_T}\right) - \exp\left(\frac{\psi_{1\min}(y_m)}{V_T}\right)\right) \tag{3.14}$$

where $E_F = \frac{\psi_{1\min}(y_m) - \psi_{1\min}(0)}{y_m}$ (3.15)

$$E_b = \frac{\psi_{1\min}(y_m) - \psi_{1\min}(t_{si})}{y_m - t_{si}} \tag{3.16}$$

E_F and E_b are the electric fields associated with the front and back surfaces of the device.

3.2.2 Modeling of Effective Conduction Path Parameter

Let us assume that $d_{eff,A}$ and $d_{eff,B}$ represent the effective conduction path parameters of the front and back regions of the channel. Using the methodology of Dubey *et al.* and Dey *et al.* [Dubey *et al.* (2011), Dey *et al.* (2008)], $d_{eff,A}$ and $d_{eff,B}$ can be expressed as

$$d_{eff,A} = \frac{\int_0^{y_m} y \exp\left(\frac{\psi_{1\min}(y)}{V_T}\right) dy}{\int_0^{y_m} \exp\left(\frac{\psi_{1\min}(y)}{V_T}\right) dy} \tag{3.17}$$

$$d_{eff,A} = \frac{\left(y_m - \frac{V_T}{E_F}\right)\exp\left(\frac{\psi_{1\min}(y_m)}{V_T}\right) + \left(\frac{V_T}{E_F}\right)\exp\left(\frac{\psi_{1\min}(0)}{V_T}\right)}{\exp\left(\frac{\psi_{1\min}(y_m)}{V_T}\right) - \exp\left(\frac{\psi_{1\min}(0)}{V_T}\right)} \tag{3.18}$$

$$d_{eff,B} = \frac{\int_{y_m}^{t_{si}} y\exp\left(\frac{\psi_{1\min}(y)}{V_T}\right)dy}{\int_{y_m}^{t_{si}} \exp\left(\frac{\psi_{1\min}(y)}{V_T}\right)dy} \tag{3.19}$$

$$d_{eff,B} = \frac{\left(t_{si} - \frac{V_T}{E_F}\right)\exp\left(\frac{\psi_{1\min}(t_{si})}{V_T}\right) - \left(y_m - \frac{V_T}{E_F}\right)\exp\left(\frac{\psi_{1\min}(y_m)}{V_T}\right)}{\exp\left(\frac{\psi_{1\min}(t_{si})}{V_T}\right) - \exp\left(\frac{\psi_{1\min}(y_m)}{V_T}\right)} \tag{3.20}$$

Now, the effective subthreshold current conduction path parameter of the device can be expressed as [Dubey *et al.* (2011), Dey *et al.* (2008)]

$$d_{eff} = \frac{I_{sf}\left|d_{eff,A}\right| + I_{sb}\left|d_{eff,B}\right|}{I_s} \tag{3.21}$$

3.2.3 Modeling of Subthreshold-Swing

Subthreshold-swing (SS) can be defined as [Dubey *et al.* (2011)]

$$SS = \left(\frac{\partial \log I_s}{\partial V_{gs}}\right)^{-1} \tag{3.22}$$

where I_s is SC of the device. Again using the methodology of Dubey *et al.* [Dubey *et al.* (2011)], swing can be expressed as

$$SS = V_T(\ln 10)\left(\frac{\partial \psi_{1\min}(y)}{\partial V_{gs}}\right)^{-1} \tag{3.23}$$

Equation (23) shows that SS is a function of y , which is undesirable since swing is a device parameter. Replacing y by d_{eff} as in Ref. [Dubey *et al.* (2011)], the SS can be finally expressed as

$$SS = V_T(\ln 10)\left(\frac{\partial \psi_{1\min}(d_{eff})}{\partial V_{gs}}\right)^{-1} \tag{3.24}$$

3.3 Results and Discussion

In this section, model results of GCDMDG MOSFETs will be compared with the corresponding results of the conventional DMDG MOSFETs and GCDG MOSFETs to express the superiority of the GCDMDG MOSFETs among all the three structures considered and already discussed in Chapter1. For the DMDG MOSFET, the uniform doping of the channel has been assumed to be the arithmetic mean of N_{a1} and N_{a2} whereas the average value of ϕ_{m1} and ϕ_{m2} has been considered as work-function of single-material-gate-electrode of the GCDG MOSFET structure in the same manner as used in Chapter 1. The drift-diffusion, CVT mobility (Lombardi Model), Fermi-Dirac carrier statistics and the standard SRH and Auger recombination models (*srh* and *aug*) have been used for simulating all the device structures in the ATLAS^{TM} 2D device simulator.

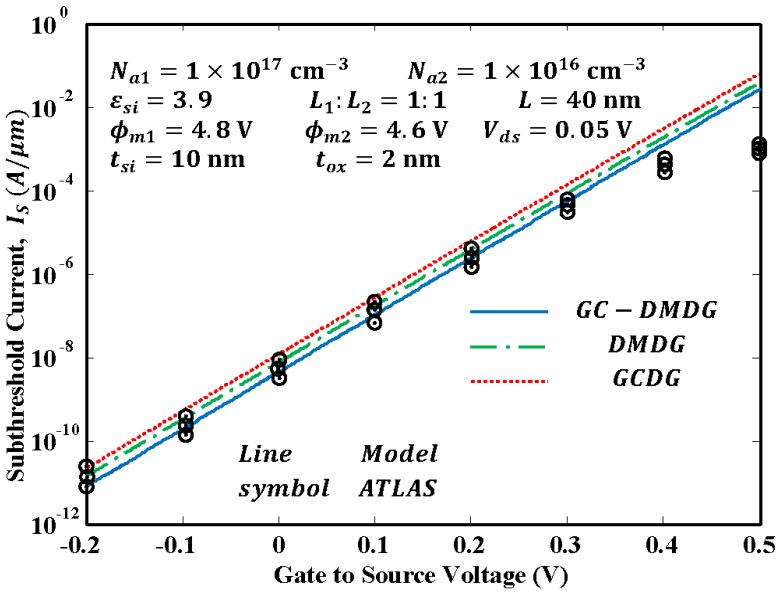

Fig. 3.2: Variation of SC with V_{gs} for the three different structures

For the three MOS structures under study, variations of SC vs V_{gs} are shown in Fig. 3.2. Note that the SC is the lowest for GCDMDG structure as compared to that of the DMDG and GCDG structures. This can be attributed to the highest source-channel potential barrier (i.e. the largest V_{th}) of the GCDMDG MOSFET due to the combined effects of higher work function of gate electrode material and higher channel doping near the source end, explained in Chapter1. Figure 3.2 also shows an increase in the SC with increasing V_{gs}. Modeling and simulation results are well agreed in the subthreshold regime (below V_{th}) as diffusion phenomenon only has been taken into account to formulate the current.

Figure 3.3 explains SC versus V_{gs} variations for different channel lengths of the GCDMDG MOSFET. It is clear from the figure that SC increases with the decrease in the channel length. This might happen due to reduced control of the gate over the channel at shorter channel lengths owing to the enhanced SCEs like DIBL thereby allowing the source and the

drain to play a dominant role in controlling the channel electric charges. Further, with increasing channel length, the slope of SC versus V_{gs} graph is increased, indicating the improved switching characteristics of the device.

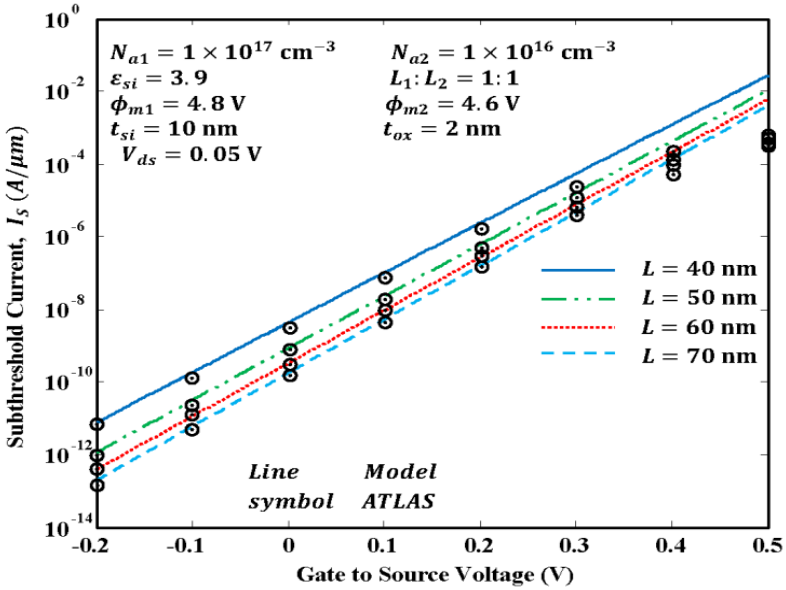

Fig. 3.3: Variation of SC with V_{gs} for GCDMDG MOSFET for different values of channel length

Variation of the SC with V_{gs} for different values of control-to-screen gate-length ratio (already described in Chapter 1) for GCDMDG MOSFET is investigated in Fig. 3.4. The higher gate-length ratio L_1/L_2 helps to reduce SC effectively, possibly due to increased V_{th} as shown in Chapter-1.

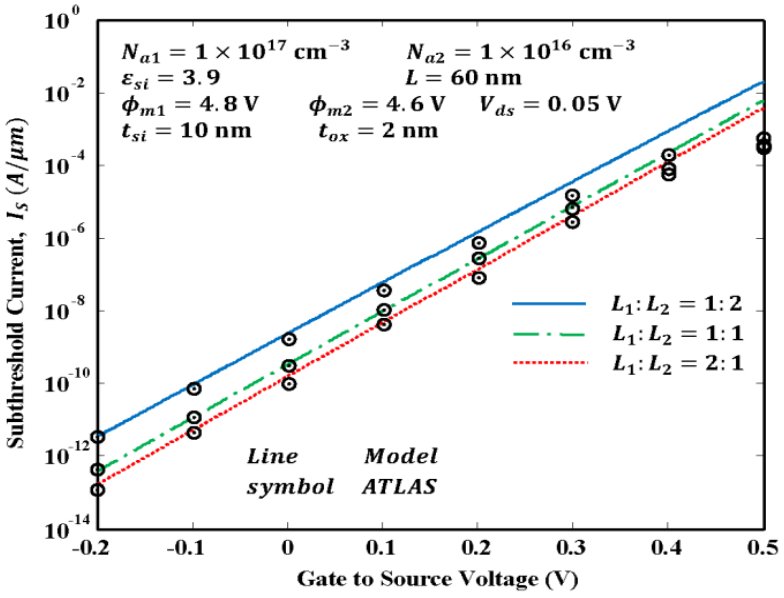

Fig. 3.4: Variation of SC with V_{gs} for GCDMDG MOSFET for different values of L_1/L_2

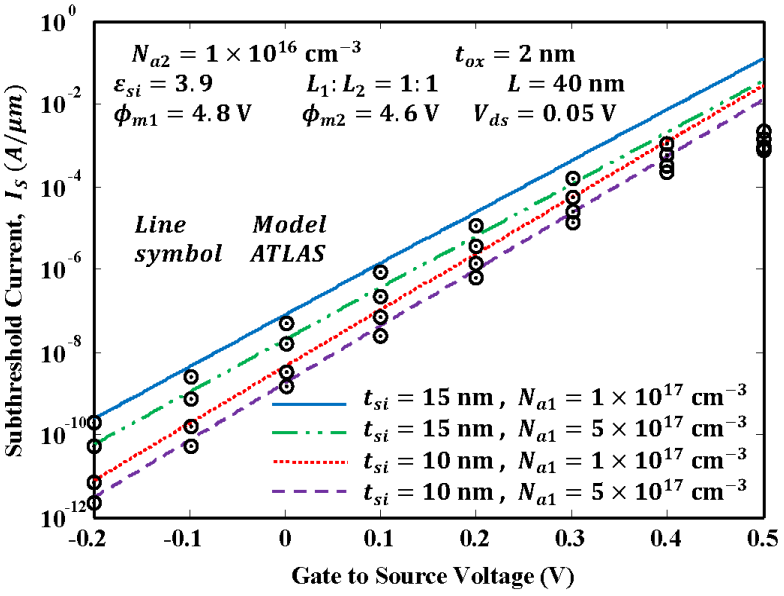

Fig. 3.5: Variation of SC with V_{gs} for GCDMDG MOSFET for different values of t_{si} and N_{a1}

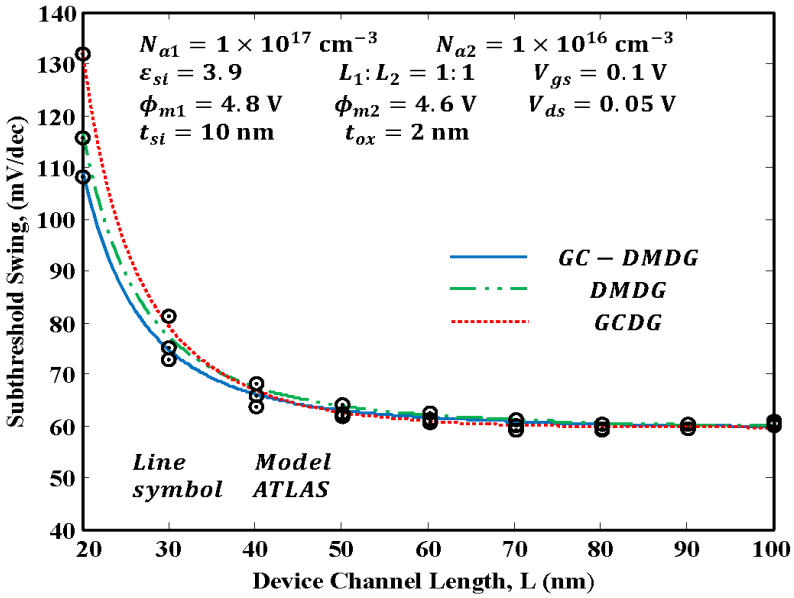

Fig. 3.6: Variation of SS with the channel length for the three different structures

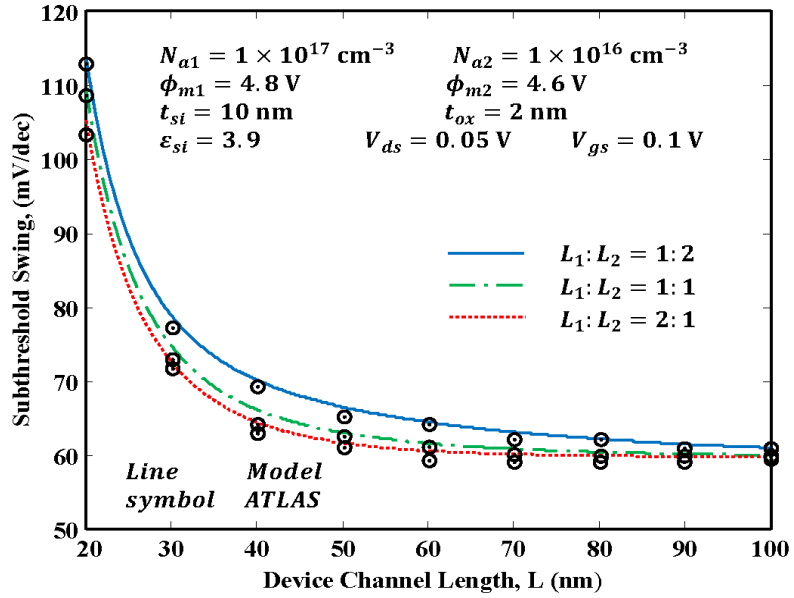

Fig. 3.7: Variation of SS with the channel length for GCDMDG MOSFET for different values of L_1/L_2

Figure 3.5 presents the effects of different values of the channel doping concentration and channel thickness on the SC versus V_{gs} plot of GCDMDG MOSFET. Since reduction in the channel doping concentration reduces the source/channel barrier height, more number of electrons starts entering from the source into the channel to raise the SC of the device. It is also clear from the figure that higher value of the channel thickness increases SC due to weak channel electrostatics (increased SCEs).

We have investigated the variation of SS for the three MOS structures under consideration as a function of device channel length in Fig. 3.6. It is observed from the figure that SS is minimum for GCDMDG MOS structure and maximum for GCDG MOS structure.

The variation of SS with device channel length for different L_1/L_2 ratio for GCDMDG structure is shown in Fig. 3.7. It can be easily observed that larger value of L_1/L_2 ratio is associated with a lower SS i.e. better switching characteristics (especially for channel lengths below 40 nm) possibly due to improved V_{th} and V_{th} roll-off as discussed in Chapter 1.

3.4 Conclusion

In this chapter, we present a two-dimensional analytical model for SC and SS of the GCDMDG MOSFETs. The superior performance of GCDMDG MOSFET over GCDG and DMDG structures has been observed in terms of smaller values of SC and SS. The effects of different device parameters like channel length, control-to-screen gate length ratio, channel thickness, doping concentration etc. have been investigated on the subthreshold characteristics of the device. The reasonably good matching of the model results with the

2D ATLAS^{TM} device simulator data, shows the validity of the model.